Robust Midsagittal Plane Extraction from Normal and Pathological 3-D Neuroradiology Images

Yanxi Liu*, *Member, IEEE*, Robert T. Collins, *Member, IEEE*, and William E. Rothfus

***Abstract*—This paper focuses on extracting the ideal midsagittal plane (iMSP) from three-dimensional (3-D) normal and pathological neuroimages. The main challenges in this work are the structural asymmetry that may exist in pathological brains, and the anisotropic, unevenly sampled image data that is common in clinical practice. We present an edge-based, cross-correlation approach that decomposes the plane fitting problem into discovery of two-dimensional symmetry axes on each slice, followed by a robust estimation of plane parameters. The algorithm's tolerance to brain asymmetries, input image offsets and image noise is quantitatively evaluated. We find that the algorithm can extract the iMSP from input 3-D images with 1) large asymmetrical lesions; 2) arbitrary initial rotation offsets; 3) low signal-to-noise ratio or high bias field. The iMSP algorithm is compared with an approach based on maximization of mutual information registration, and is found to exhibit superior performance under adverse conditions. Finally, no statistically significant difference is found between the midsagittal plane computed by the iMSP algorithm and that estimated by two trained neuroradiologists.**

***Index Terms*—Medical image analysis, midsagittal plane, pathological neural image analysis, robust estimation, symmetry detection.**

I. Motivation

NORMAL human brains exhibit an approximate bilateral symmetry with respect to the interhemispheric (longitudinal) fissure bisecting the brain, known as the anatomical **midsagittal plane** (MSP). However, human brains are almost never perfectly symmetric [5], [6], [10]. Pathological brains, in particular, often depart drastically from bilateral symmetry. For effective pathological brain image alignment and comparison (e.g., [5], [16]), it is most desirable to define a *plane of reference* that is invariant for symmetrical as well as asymmetrical brain images, and to develop algorithms that capture this reference plane robustly.

We define an *ideal midsagittal plane* (iMSP) as *a virtual geometric plane about which the three-dimensional (3-D) anatomical structure captured in the given neuroimage presents maximum bilateral symmetry*. Factors that challenge the robustness of an iMSP extraction algorithm include: 1) the intrinsic factor: the brain and the skull being imaged can be either bilaterally symmetric or asymmetric. Brain asymmetry can be caused by any combinations of normal brain asymmetry, abnormal tissue intensity alteration, and mass effect. Abnormal tissue intensity alteration can happen due to, e.g., a nonhemorrhagic stroke as shown in Fig. 1(a). Mass effect can be caused by virtue of swelling or space occupying lesions, e.g., a tumor as shown in Fig. 1(c). 2) the extrinsic factor(s): the volumetric neuroimage can be anisotropic, and/or unevenly sampled[1] ; and initial alignment inconsistencies and artifacts/noise can be introduced during the imaging process. The goal of our work is to extract the iMSP from a clinical 3-D neuroimage while tolerating both intrinsic and extrinsic factors.

The well-known Talairach framework is an anatomical landmark-based approach to define a 3-D brain coordinate system [30]. The principal orthogonal axes in the Talairach framework are determined by a line passing through the anterior and posterior commissures, called the AC–PC line, a line going through the posterior margin of the anterior commissure and perpendicular to the AC–PC line, called the (VAC)[2] line, and the interhemispheric sagittal plane (referred to as the midline in [30, p. 5]). Besides the intrinsic and extrinsic factors mentioned above, patient image to Talairach framework registration is difficult to achieve automatically due to its reliance on precise location of 3-D anatomical image features that may not be obviously identifiable. Furthermore, when the interhemispheric sagittal plane no longer lies on a flat surface due to normal or pathological deformation [Fig. 1(c)], the interhemispheric medial *plane* is ill-defined. In contrast, the iMSP is based on global geometry of the head and can be found using low-level image processing techniques. It remains well-defined in pathological brains, forcing a virtual left–right separation consistent with the location where an *ideal* midsagittal plane would have been if no tissue deterioration or mass effect had occurred [Fig. 1(b) and (d)]. Automatic extraction of the iMSP, at least, can provide an initial estimate for the automation of Talairach framework alignment in pathological neuroimages.

Designing a robust algorithm that handles clinical neuroimages with pathologies originates from our desire to facilitate on-line clinical image database indexing and retrieval for

Manuscript received September 28, 1999; revised January 11, 2001. This work was supported in part by the Allegheny–Singer Research Institute under Prime Contract through the Advanced Technology Program of the National Institute of Standards and Technology (NIST 70NANB5H1183). The Associate Editor responsible for coordinating the review of this paper and recommending its publication was D. Hawkes. *Asterisk indicates corresponding author.*

*Y. Liu is with the Robotics Institute, Carnegie Mellon University, 5000 Forbes Ave., Pittsburgh, PA 15213 USA (e-mail: yanxi@cs.cmu.edu).

R. T. Collins is with the Robotics Institute, Carnegie Mellon University, 5000 Forbes Ave., Pittsburgh, PA 15213 USA.

W. E. Rothfus is with the Department of Radiology, Division of Neuroradiology, University of Pittsburgh Medical Center, Pittsburgh, PA 15213 USA.

Publisher Item Identifier S 0278-0062(01)02777-X.

[1]Here, "anisotropic" means that the image voxel shape is not a cube, e.g., the slice thickness can be 10 mm while pixel size on each slice is $\leq 1 \times 1$ mm^2. "Unevenly sampled" means that there can be more than one slice thickness in one 3-D image, e.g., some slices have thickness 5 mm and some 10 mm (Table II). These are more common in computed tomography (CT) images.

[2]The line that is vertically traversing the posterior margin of the anterior commissure. This line is the basis for the vertical frontal plane [30].

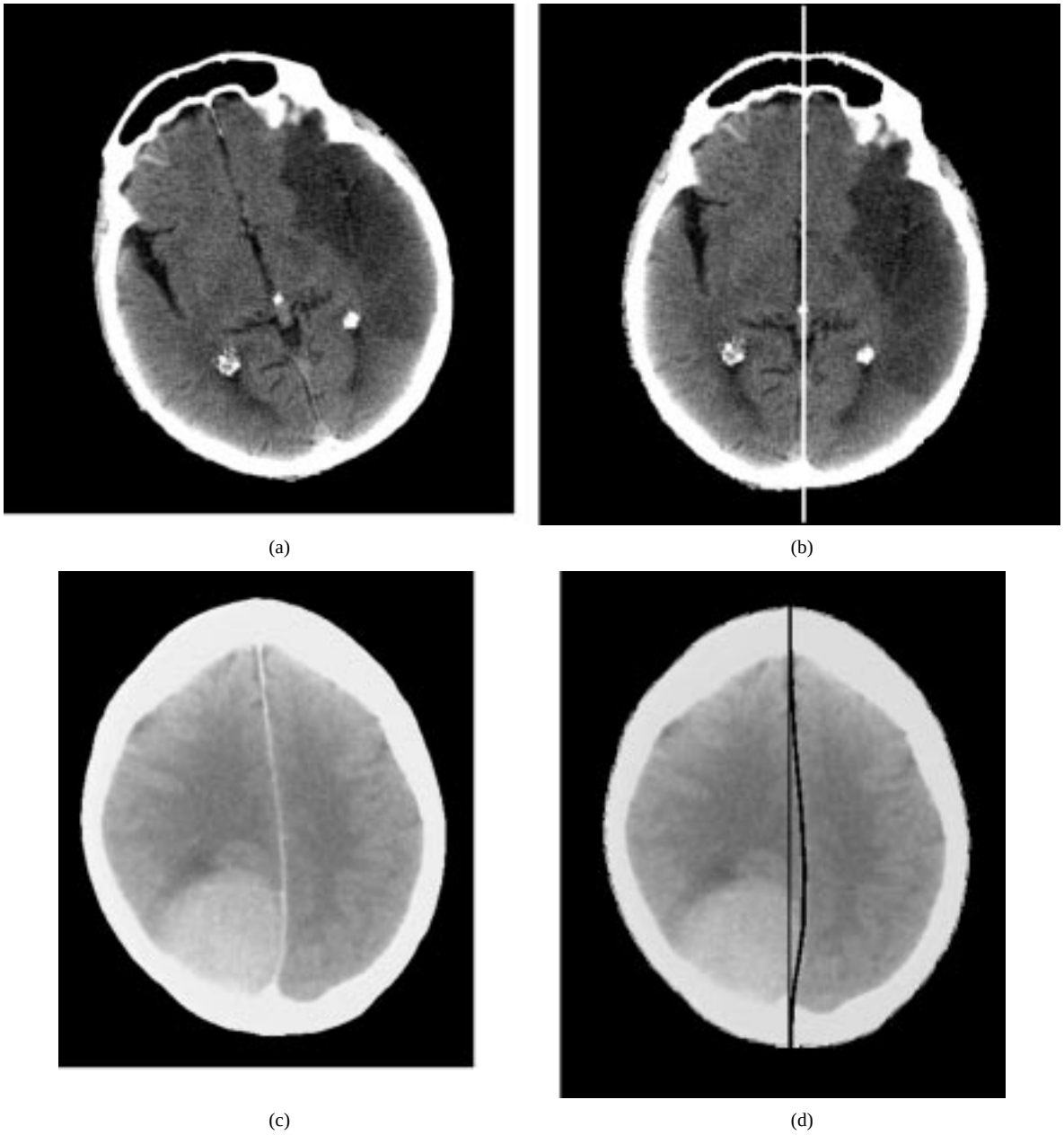

Fig. 1. (a) Nonspace-occupying lesion (infarct). (b) The intersection of the iMSP and the given two–dimensional (2-D) axial slice. (c) An axial brain slice with deformed midline due to a tumor. (d) The intersection of the extracted iMSP with the same 2-D brain slice (straight line), and the deformed midline (curved line) captured by a "snake" active contour.

real-time medical image consultation [16], [17]. This effort fills a gap in medical image analysis algorithms, as stated in [8], "To date, all too often image analysis algorithm development ignores the analysis of different abnormal, pathological or disease states." Our iMSP extraction algorithm is designed for and tested on both normal and pathological, 3-D CT or magnetic resonance (MR) neuroimages. The iMSP is robustly determined via an edge-based geometric approach applied to both axial and coronal 2-D slices of the given 3-D image. The algorithm has been applied to 130 clinical volumetric images and tested on both real and synthetic images with ground truth. Breakdown points of the iMSP extraction algorithm are found by varying brain orientation, lesion size, noise level, and bias field. The iMSP algorithm compares favorably with a method based on maximization of mutual information. We also find no significant difference between the iMSP orientations estimated by our iMSP algorithm and those hand-picked by two neuroradiologists.

In Section II, we review existing work on automatic MSP extraction. In Section III, we present the underlying geometry of the midsagittal plane, together with an edge-based, robust estimation algorithm for iMSP extraction. Sample experimental results are shown in Section IV, followed in Section V by evaluation on real and synthetic images, and an analysis of performance with respect to human experts. In Section VI, we discuss issues in model accuracy, speed, and applications related to the iMSP extraction algorithm. Finally, in Section VII, we present a brief summary and discussion of future work.

II. Related Work

Existing work under the general topic of symmetry detection, and the specific topic of neuroimage MSP extraction, can be described and compared in terms of four main aspects:

A. The Goal

The goal of most symmetry detection algorithms [7], [9], [19], [22], [26], [29], [32], [34] is to find the symmetry point/line/plane of an object that is known to be nearly symmetrical. Similarly, the goal of most MSP detection algorithms [1], [11], [20], [2], [12] is to locate the plane of reflection of a nearly symmetrical brain image. It must be realized, however, that MSP means different things to different algorithms. The MSP can be defined as the plane about which there is most structural symmetry of the brain, skull or head, as the plane that best fits the interhemispheric fissure, or even as the plane determined by a particular image processing routine. That is, the definition of an MSP can be either feature-based (e.g., the interhemispheric fissure) or image-based (using a similarity measure computed from image properties).

B. The Approach

Several existing algorithms designed specifically for MSP extraction are listed in Table I. These approaches can be further divided into two gross categories: feature-based versus image similarity-based. The MSP extraction algorithms are compared in terms of image modality, image dimension,[3] and feature/similarity measurement.

Feature-based methods include the work of [2] and [11]. In [2], the author uses a Hough transform to find straight lines—the longitudinal fissure line on the upper portion of the brain. In [11], the fissure line is extracted from each slice using linear snakes and then a plane is found using orthogonal regression. Both methods encounter the same problem when the longitudinal fissure line departs drastically from a straight line due to mass effect.

Image similarity-based approaches include the rest of the references listed in Table I. The authors of [12] use cross correlation of intensity images as the similarity measure applied on 2-D images, and report that the method is sensitive to brain asymmetry. The work in [20] uses a method called stochastic sign change to determine the similarity of two images. The authors report their surprise at finding that the algorithm, developed for normal brains, is also capable of finding the correct MSP on certain asymmetrical, pathological brains [on simulated positron emission tomography (PET) images]. Their results require accurate initial alignment of the head using a guiding laser beam. The most recent work on MSP extraction reported in this journal is [1]. The authors evaluate a candidate MSP using the cross correlation of two intensity vectors, each containing voxels from one side of the current estimated MSP. The authors report that the method is highly sensitive to asymmetry. More recently, Smith and Jenkinson [27] presented an algorithm for finding symmetry axes in partially damaged, asymmetrical images of various modalities. They use the ratio of intensity profiles along an estimated normal line at each voxel for determining the optimal symmetrical plane. Though it is basically an intensity-based method, a preprocessing step is suggested for images with strong bias field to distill the edge information. No quantitative evaluations have yet been given, and the computation is very expensive. Most recently, Prima *et al.* report on an MSP extraction algorithm for 3-D neuroimages which finds a plane that maximizes the bilaterally symmetric matching for each voxel examined in a specific-sized block [21]. The similarity is measured by correlation. No images with significant asymmetry or pathology are shown.

[3]Here, "2-D images" means each 2-D brain slice is treated independently, and "3-D images" means volumetric image data.

TABLE I
Existing Work on MSP Detection

Author Reference Year	Image Modality	Image Dimension	Feature Measure
Brummer [2] 91	MR	2D	edge Hough transform
Guillemaud et al [11] 95	MR	3D	interhemispheric fissure, snake
Author Reference Year	**Image Modality**	**Image Dimension**	**Image Similarity Measure**
Junck et al [12] 90	PET SPECT	2D	intensity cross correlation
Minoshima et al [20] 92	PET	3D	stochastic sign change
Ardekani et al [1] 97	MR,PET	3D	intensity cross correlation
Liu et al [15, 13] 98 00	MR, CT	2D or 3D	edge cross correlation least-median dist
Smith & Jenkinson [27] 99	CT,MR,PET SPECT	3D	ratio of intensity profiles
Prima et al [21] 00	CT,MR,PET SPECT	3D	intensity cross correlation

Maximization of mutual information theory, another intensity-based approach, has been applied successfully to multimodal brain registration under both rigid and affine transformations [18], [28], [31], [33]. The iMSP could be extracted using mutual information by registering a 3-D brain volume with a reflected version of itself to find the best plane of reflection. We have experimented with this approach (see Section V). Although it is relatively insensitive to the introduction of simulated spherical lesions, due to the global nature of the processing, the method is more sensitive than our algorithm to degradation in signal to noise ratio due to random noise, and very sensitive to intensity bias fields.

C. The Evaluation

The evaluations given in previous papers on MSP extraction are based on visual inspections by the authors, or on results from nonpathological neuroimages only. No quantitative validations are provided systematically. The algorithm in [20] is tested with images containing simulated spherical lesions on simulated PET images, but the authors did not explore failure modes of the algorithm. Synthetic MR images are used for testing in [21] but results are reported for successful experiments alone.

D. The Data

Unlike finely sampled research data containing the entire brain, as is used by most neurological image understanding researchers, unevenly sampled, anisotropic clinical images

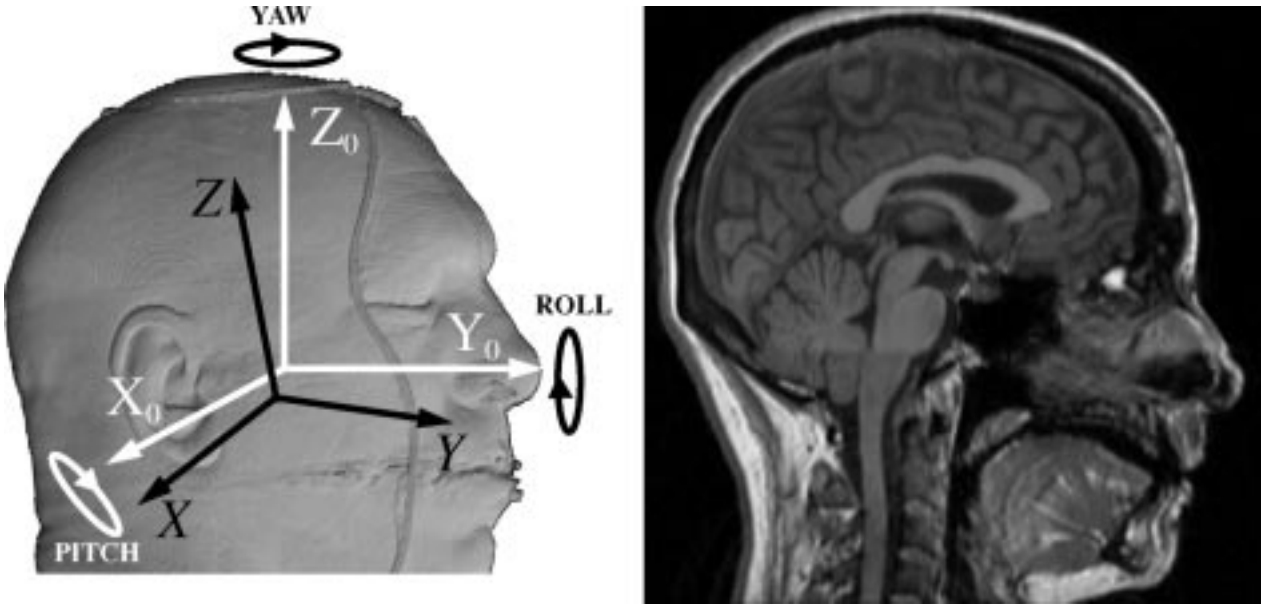

(a) (b)

Fig. 2. (a) Ideal head coordinate system $X_0Y_0Z_0$ versus the imaging coordinate system XYZ. The iMSP algorithm finds the transformation between planes $X_0 = 0$ and $X = 0$. Rendered head courtesy of the Visible Human Project. (b) A midsagittal plane ($X_0 = 0$) automatically extracted using our iMSP extraction algorithm.

make it difficult to infer 3-D structure by simply interpolating the missing data between slices. The absence of information between slices in turn makes it difficult to use volumetric intensity-based approaches. Little work has been reported on effective MSP extraction approaches for dealing with clinical images and pathological cases, both of which are of great importance in applied medical image analysis.

Our work, reported in this paper, differs from previous approaches as follows:

1) *The Goal:* our goal is to find the iMSP both in normal (statistically more symmetrical) and especially in pathological (statistically more asymmetrical) neuroimages;
2) *The Approach:* the approach taken is edge-based rather than intensity-based, and decomposes symmetry plane extraction in a volume into discovery of 2-D symmetry lines on each slice, followed by a robust fitting of a 3-D plane.
3) *The Evaluation:* the algorithm is evaluated on clinical CT and MR data, and quantitatively tested using synthetic images and real images with ground truth provided by human experts;
4) *The Data:* the algorithm is applied to clinical image data ranging from dense MR images (voxel dimension close to $1 \times 1 \times 1$ mm^3) to CT images that are anisotropic (e.g., voxel dimension $0.5\times 0.5 \times 10$ mm^3) and unevenly sampled (e.g., 5-mm and 10-mm slice thicknesses exist in one 3-D image).

III. 3-D Midsagittal Plane Extraction

Neuroradiology scans are in nature 3-D volumetric data expressed as a stack of 2-D images. In this section, we present geometric analysis and a working algorithm for extracting the iMSP from these scans.

We define an *ideal head coordinate system* centered in the brain with positive X_0, Y_0, and Z_0 axes pointing to the right, anterior and superior directions, respectively (Fig. 2, white coordinate axes). With respect to this coordinate system, the plane $X_0 = 0$ is defined to be the iMSP of the brain: *a virtual geometric plane about which the 3-D anatomical structure presents maximum bilateral symmetry*. Ideally, a set of *axial (coronal)* slices is cut perpendicular to the $Z_0(Y_0)$ axis, and the intersection of the iMSP with each slice appears as a vertical line on the slice.[4]

In clinical practice, however, the *imaging coordinate system* XYZ [Fig. 2(a)], black coordinate axes) differs from the ideal coordinates due to positioning offsets (translations) and rotation of the head introduced so that a desired volume can be better imaged. The orientation of the imaging coordinate system differs from the ideal coordinate system by three rotation angles, pitch, roll and yaw, about the X_0, Y_0, and Z_0 axes, respectively [Fig. 2(a)]. The imaging coordinate system can also have a nontrivial translation offset. The goal of an iMSP algorithm is to find the transformation between the two planes $X_0 = 0$ and $X = 0$.

A. Geometry of the iMSP

Under the *imaging coordinate system*, the iMSP can be represented as

$$aX + bY + cZ + d = 0 \tag{1}$$

where (a, b, c) is a vector describing the plane normal and $d/\sqrt{a^2 + b^2 + c^2}$ is the perpendicular distance of the plane from the origin. The parameters (a, b, c, d) can be scaled by an arbitrary, nonzero amount. For the rest of this section, we assume that they have been scaled so that $\sqrt{a^2 + b^2} = 1$. Now

[4]The analysis given to axial slices from now on can be applied also to coronal slices (cut along the Y axis) with corresponding symbols changed: "Z" to "Y."

consider the ith axial slice, represented by the plane equation $Z = Z_i$. The 2-D axis of bilateral symmetry on the ith slice is the intersection of the above two planes

$$aX + bY + (cZ_i + d) = 0. \tag{2}$$

This is the equation of a 2-D line (θ_i, ρ_i) in the XY plane, having line orientation

$$\theta_i = \arctan(b/a) \tag{3}$$

and 2-D perpendicular offset to the point $X = 0, Y = 0, Z = Z_i$

$$\rho_i = cZ_i + d. \tag{4}$$

We can make two immediate observations from (2). First, since the iMSP is assumed to be a planar surface, the orientation angle $\theta_i = \arctan(b/a)$ of each 2-D symmetry axis should be the same for all slices regardless of their Z_i position [Equation (3)]. Secondly, the offset ρ_i of the symmetry axis on slice $Z = Z_i$ is linearly related to Z_i as a function of plane parameters c and d [see, (4)]. Therefore, given the translational offset of at least two symmetry axes on different slices, we can compute c and d by solving a set of linear equations. These observations form the basis for the iMSP extraction algorithm described in the next section.

A different way to express the $X_0 = 0$ plane in the imaging coordinates is to view each point on the plane as being transformed from $X_0Y_0Z_0$ to XYZ by an unknown rotation $\mathcal{R} = \mathbf{yaw}(\theta)\mathbf{roll}(\phi)\mathbf{pitch}(\omega)$ and displaced by an unknown translation ΔX_0, ΔY_0, and ΔZ_0. Specifically, points in the ideal coordinate system are mapped into the imaging coordinate system by the transformation

$$\begin{bmatrix} X \\ Y \\ Z \end{bmatrix} = \begin{bmatrix} c\phi c\theta & c\theta s\omega s\phi - c\omega s\theta & c\omega c\theta s\phi + s\omega s\theta \\ c\phi s\theta & c\omega c\theta + s\omega s\phi s\theta & c\omega s\phi s\theta - c\theta s\omega \\ -s\phi & c\phi s\omega & c\omega c\phi \end{bmatrix} \cdot \begin{bmatrix} X_0 \\ Y_0 \\ Z_0 \end{bmatrix} + \begin{bmatrix} \Delta X_0 \\ \Delta Y_0 \\ \Delta Z_0 \end{bmatrix} \tag{5}$$

where $c\theta \equiv \cos\theta$, $s\theta \equiv \sin\theta$, and so on. The iMSP $X_0 = 0$ can be rewritten in terms of the imaging coordinates as

$$\cos\phi\cos\theta X + \cos\phi\sin\theta Y - \sin\phi Z - (n.\Delta) = 0 \tag{6}$$

where $n = (\cos\phi\cos\theta, \cos\phi\sin\theta, -\sin\phi)^T$ is the unit normal vector of the plane and $\Delta = (\Delta X_0, \Delta Y_0, \Delta Z_0)^T$. Dividing by $\cos\phi$ provided[5] $\text{abs}(\phi) \neq 90°$, and comparing with (1)

$$\begin{aligned} &a = \cos\theta \qquad b = \sin\theta \qquad c = -\tan\phi \\ &d = -(n.\Delta)/\cos\phi. \end{aligned} \tag{7}$$

That is, the shared angle $\theta = \theta_i = \arctan(b/a)$ of each axial slice is actually the yaw angle of the head's imaging coordinate system. Furthermore, the roll angle ϕ can be determined from the offsets of the 2-D symmetry axes on the set of slices by solving a linear system of equations specified in (4). Note from (4) and (7) that when the roll angle ϕ is zero, plane parameter $c = 0$ and, thus, all 2-D symmetry axes have the same offset $\rho_i = d$ regardless of Z_i; otherwise, ρ_i varies linearly from slice to slice. Finally, the quantity $(-d\cos\phi)$ measures the displacement of the imaging coordinate system in the direction normal to the iMSP.

[5]This is a modest geometric restriction on the roll angle. If the roll angle were to approach 90°, we would be dealing with *sagittal* rather than axial slices.

B. Symmetry Plane Extraction Algorithm

The geometric results from the previous section have been used to develop an algorithm for automatically extracting the iMSP of neuroimages. The input is a set of slices from an axial (coronal) CT or MR brain scan, along with the associated voxel dimensions. The output is an estimate of the head's yaw and roll angles, and the best-fit iMSP, represented as a set of 2-D symmetry axes superimposed on each slice.

1) Preprocessing Each Slice: The format of the images we receive varies from scanned-in 8-bit gray images with an average size of 650 × 550, to 16-bit DICOM3 format raw images with a standard size of 512 × 512 or 256 × 256. The number of slices in each 3-D image ranges from nine to 187, and slice thickness/space ranges from 1.2 to 10 mm. Sometimes a 3-D image contains more than one slice thickness (see Table II). Although each image is dominated by the patient's head, some images contain additional clutter superimposed on the slice in the form of patient data, acquisition parameters, and the physical cross section of the head-rest (Fig. 9). We have developed a simple procedure for preprocessing each slice to remove this clutter, and thereby isolate just the head region, by adaptively thresholding to produce a binarized image and choosing the largest connected region in that image (details can be found in [14]).

We would like the iMSP extraction algorithm to operate on the 3-D structure of the brain and bony regions, and not be unduly influenced by large homogeneous intensity regions, or even the raw intensity values themselves. For this reason, we first extract binary edges from each slice, and perform all further processing on these edge images. Each edge image is created by convolving with a Laplacian and marking zero crossings. Any similar binary edge extraction technique, such as the Canny edge detector [3], would yield similar results.

Finally, we wish the edge information to capture only gross anatomical structures of the brain and skull, and to ignore fine details and intensity fluctuations. This is achieved by spatial filtering of the images before edge extraction. Specifically, images are repeatedly reduced (smoothed and subsampled) by a factor of 2 until the shortest side is between 32 and 64 pixels in length. Edge extraction is performed on this reduced image, so that only large-scale anatomical boundaries are found. In addition to filtering out fine details, the resulting reduction in image size also speeds up the subsequent processing steps.

2) Estimating Symmetry Axis Orientation θ_i for Each Slice: Geometric reasoning in Section III-A tells us that each 2-D symmetry axis should have the same orientation θ, which corresponds to the yaw angle of the patient's head. The algorithm begins by extracting an estimate of this angle from each 2-D axial slice. These estimates are later combined to form a single best estimate.

TABLE II
A SAMPLE OF INPUT 3-D IMAGE DATA

Set	Modality	Orientation	Matrix	Voxel (mm^3)	Pathology
3	CT enhanced	axial	686x550x33	0.5x0.5x5 (1-15) 0.5x0.5x10 (16 - 33)	right parietal/occipital meningioma
5	MR	coronal	256x256x123	0.9375x0.9375x1.5	Normal
17	CT	axial	686x550x9	0.5x0.5x10	Right thalamic acute bleed
58	CT	axial	678x542x17	0.5x0.5x5 (1-9) 0.5x0.5x10 (10-17)	Frontal astrocytoma high grade glial tumor
82	MR	sagittal	256x256x124	0.9375 x 0.9375 x 1.5	Left parasella meningioma
87	MR	sagittal	256x256x124	0.9375 x 0.9375 x 1.5	right frontal astrocytoma
89	MR	sagittal	256x256x124	0.9375 x 0.9375 x 1.5	Left frontotemporal astrocytoma
91	MR	axial	176x236x187	0.98x0.98x1.2	Normal
109	CT	axial	512x512x21	0.4395x0.0.4395x5 (1-10) 0.4395x0.4395x8 (11-21)	Left parietal infarct
110	CT	axial	512x512x24	0.4297x0.4297x5	Normal
112	CT	axial	256x256x20	0.8672x0.8672x5 (1-11) 0.8672x0.8672x8 (12-20)	Right occipital infarct

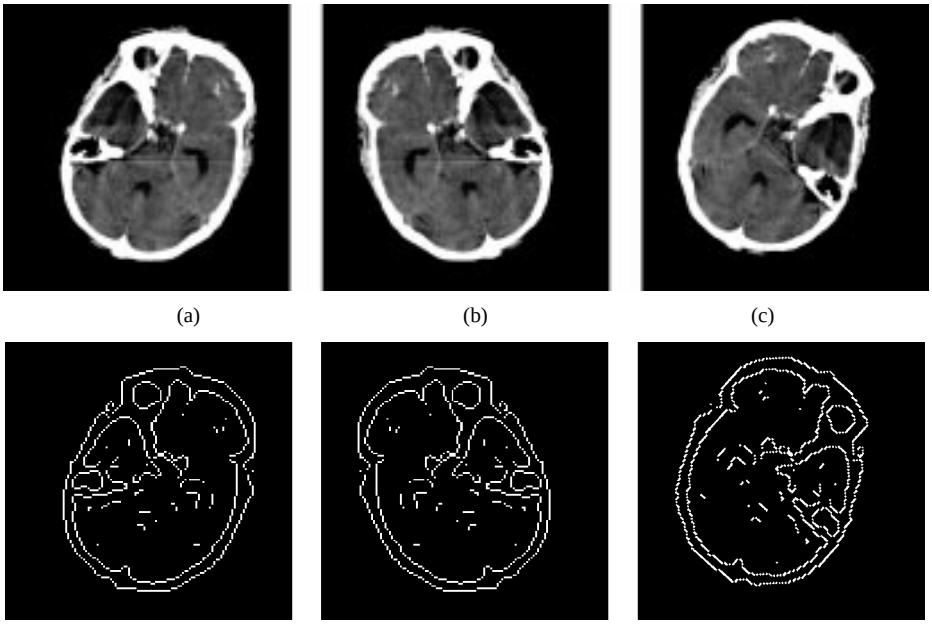

Fig. 3. (a) A CT axial head image S_i. (b) The vertically reflected image $ref_V(S_i)$. (c) The rotated reflected image $rot(ref_V(S_i),\ 2\theta)$. (d)-(f) The corresponding edge images. Note that if S_i is oriented with angle θ, $ref_V(S_i)$ has angle $-\theta$, thus, we must rotate by 2θ to bring it into alignment with S_i.

Recall the definition of bilateral symmetry: a reflection of a bilaterally symmetric image S_i about its symmetry axis produces a figure $ref(S_i)$ that is approximately identical to S_i. Therefore, the orientation of the reflection line that maximizes the cross correlation between the original image and its reflection is searched for. First, the image S_i is reflected about the current vertical center line, which is the intersection of the 2-D slice with the $X = 0$ plane in imaging coordinates, to produce a new image $ref_V(S_i)$. This has the effect of reflecting the corresponding 3-D volumetric image with the $X = 0$ plane (Fig. 2). If the reflection axis of S_i is oriented $\theta°$ from vertical, then the symmetry axis of $ref_V(S_i)$ will be oriented $-\theta°$ from vertical, regardless of where it appears in the image (Fig. 3). Therefore, to evaluate a candidate orientation θ_j, we rotate $ref_V(S_i)$ by $2\theta_j$ about the center of the image, cross correlate with the original image S_i, and record the maximum correlation value. Formally, the maximum cross-correlation value M_{S_i,θ_j} for brain slice i at angle θ_j can be expressed as $M_{S_i,\theta_j} = \max\{C_{S_i,\theta_j}(x, y)\}$, where the correlation score surface C_{S_i,θ_j} is expressed as a function of the 2-D location (x, y)

$$C_{S_i,\theta_j}(x, y) = \sum_{x'=1}^{x_0} \sum_{y'=1}^{y_0} S_i'(x' - x, y' - y) \times S_i(x', y')$$

and

$$S_i'(x, y) = rot(ref_V(S_i), 2\theta_j) \tag{8}$$

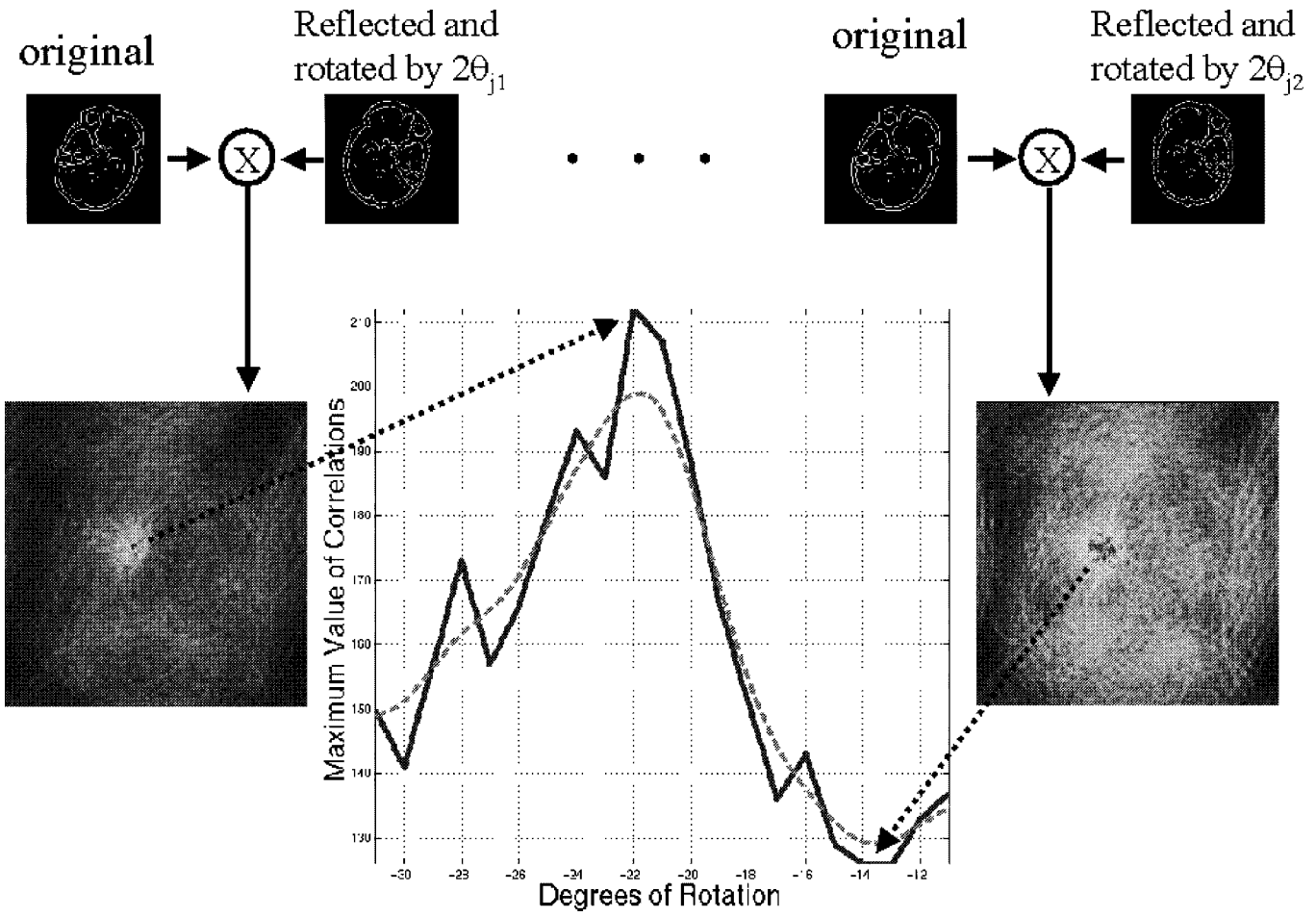

Fig. 4. Using pairs of edge images to find the best correlation value for each given rotation angle. The cross-correlation surfaces, C_{S_i,θ_j}, are shown for $\theta_{j_1} = -22°$ and $\theta_{j_2} = -14°$. The brightest point indicated the highest correlation score. Note: the correlation values have been rescaled for better viewing. Also shown is a plot of the maximum cross correlation, M_{S_i,θ_j}, between images $rot(ref_V(S_i),\ 2\theta_j)$ and S_i, for θ_j in $[-31,\ -11]$ ° sampled at every 1°.

$$size(S_i) = size(S_i') = [x_0,\ y_0] \tag{9}$$

$$x \in [-x_0,\ x_0], \qquad y \in [-y_0,\ y_0] \tag{10}$$

$$S_i'(x'-x,\ y'-y) = 0 \quad \text{when}$$
$$x' - x \notin [1, x_0] \quad \text{or} \quad y' - y \notin [1, y_0]. \tag{11}$$

The 2-D cross-correlation result C_{S_i,θ_j} is a 2-D array that is double the size of the original image in both X and Y dimensions (Fig. 4). Elements in the array contain correlation values for all possible horizontal and vertical disparities between the original image and the rotated reflected image; therefore, this method determines the orientation of the symmetry axis regardless of the translation of that axis in the image.

In most instances, a single, well-defined peak occurs in the cross-correlation surface C_{S_i,θ_j} (Fig. 4). The global maximum correlation value M_{S_i,θ_j} is recorded to represent the "score" of angle θ_j as an estimate of the unknown symmetry axis orientation. Such correlation scores are evaluated for multiple candidates θ_j within a range of possible symmetry axis orientations, to acquire a plot of correlation scores versus angles (Fig. 4). Since cross correlations must be performed for many different candidate angles, the correlation is performed in frequency space for greater efficiency. Note that the Fourier transform $\mathcal{F}$ commutes with rotations and vertical reflections, so that we only have to compute the Fourier transformation of S_i once—the flipped and rotated versions can be generated

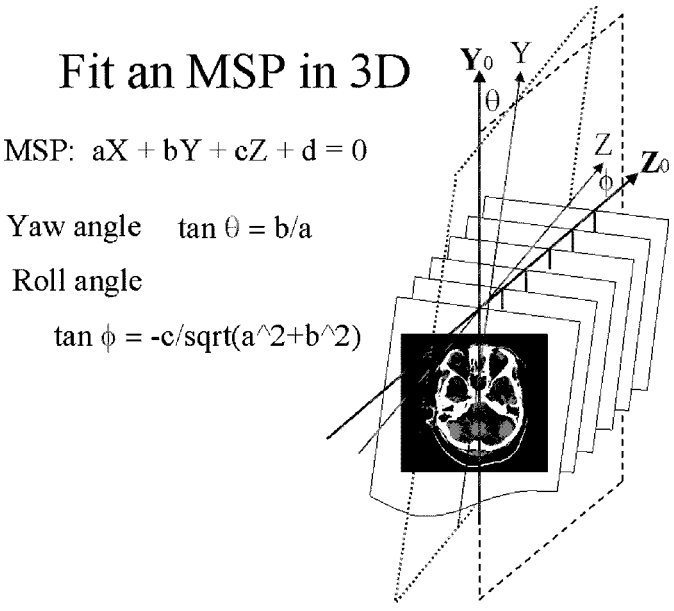

Fig. 5. Fitting the iMSP through a set of midlines in three dimensions.

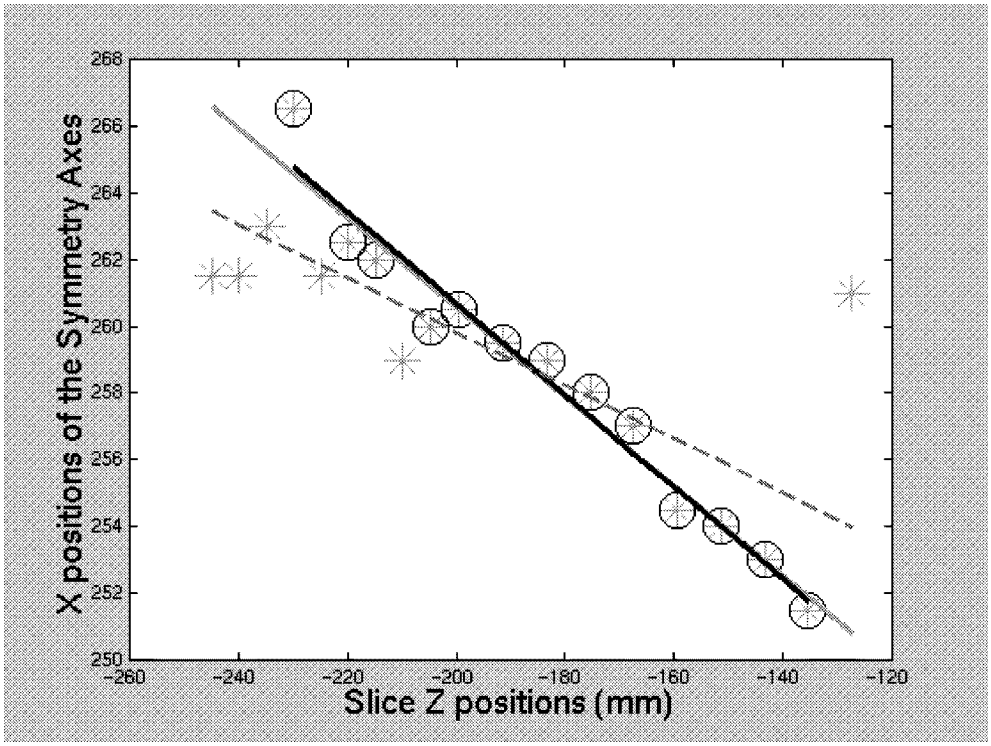

Fig. 6. Fitting the iMSP to a set of 2-D slices [one 2-D slice is shown in Fig. 1(a)]. The computed yaw angle is 21°. The stars without circles denote outlier points found and excluded from the fitting, while the stars with circles are the remaining inliers. The solid grey line is the least-median of squares line and the shorter black line is the least-squares iMSP line fit after discarding outliers. The dashed line is the MSP that would have been estimated by least-squares if outliers had not been removed.

directly in frequency space by flipping and rotating the transformed image $\mathcal{F}(S_i)$. That is

$$C_{S_i,\theta_j} = \text{XCorr}(S_i, rot(ref_V(S_i), 2\theta_j)) = \mathcal{F}^{-1}(\mathcal{F}^*(S_i) rot(ref_V(\mathcal{F}(S_i)), 2\theta_j))$$

where $\mathcal{F}^*(S_i)$ is the complex conjugate of the Fourier transform of S_i and F^{-1} is the inverse Fourier transformation [23], [25].

After testing all required angles θ_j, the one that yields the largest correlation score could be chosen as the estimate θ_i of the best symmetry axis orientation for slice S_i. That is, $\theta_i = \arg\max(M_{S_i,\theta_j})$.Since the candidate angles θ_j are coarsely sampled (say every 1°), a more precise estimate is obtained by first smoothing the correlation score versus angle curve and then finding the peak of the smoothed curve to sub-pixel precision (Fig. 4).

3) Combining $\theta_1, \ldots, \theta_m$ into a Single MSP Yaw Angle $\hat{\theta}$: Since all brain slices in the scan should have the same 2-D symmetry axis orientation, it is necessary to combine results θ_i from each slice to produce a reliable cumulative estimate $\hat{\theta}$ of the yaw angle θ for the given 3-D image. Simply taking the mean value of the θ_i would be susceptible to outliers in the computed data. Instead, we treat this as a robust estimation problem with one parameter (the yaw angle) and n sampled points, each of which is computed from one of the n 2-D slices.

First, the median of the sample values is found, and a *robust standard deviation*, $\hat{\sigma}$, is computed using the median of the absolute values of the residuals r_i

$$\hat{\sigma} = 1.4826[1 + 5/(n-p)] * median|r_i|. \quad (12)$$

The constant 1.4826 is a coefficient to achieve the same efficiency as a least-squares estimator in the presence of only Gaussian noise, p is the dimension of the parameter vector (in our case $p = 1$), and n is the number of samples. This is a standard formula from robust statistics [35]. The distribution of inliers is assumed to be Gaussian; there is no assumption on the distribution of outliers, except that they are located far away from the median. In our implementation, sample points falling 3 times the robust standard deviation from the median (median $\pm 3\hat{\sigma}$) are removed to filter outliers. The rest of the points (the inliers) are used to compute yaw angle using a biased, weighted mean estimator. For brain slice i, the exact form of weight used in our experiment is $w_i = (n - i + 1)^2$. The bias serves to give lower brain slices more weight. We have observed that the lower brain slices usually produce a "peakier" C_{S_i,θ_j} curve because the slices lower in the brain contain complex bilateral bony structures in axial slices (similarly, the frontal slices in coronal slices), while slices higher in the brain become ovals or even near-circular at the top of the head.

4) Estimating Symmetry Axis Offset ρ_i for Each Slice: Having computed a yaw angle estimate $\hat{\theta}$ that best describes the shared orientation of each 2-D bilateral symmetry axis, each image S_i is rotated by an angle $-\hat{\theta}$ so that its symmetry axis should be oriented vertically in the image. That image is then cross correlated with a vertical reflection of itself. The column C of the correlation image where the highest cross-correlation value occurs is used to compute the value of offset $\rho_i = C/2$ for that slice.

5) Computing the iMSP and Roll Angle from $\hat{\theta}$ and Offsets $\rho_1, \ldots, \rho_n$: To completely specify the iMSP involves com-

puting estimates for the plane parameters (a, b, c, d) from (1). From (7) it was seen that, given $\hat{\theta}$, we can already compute two parameter estimates $\hat{a} = \cos\hat{\theta}$ and $\hat{b} = \sin\hat{\theta}$. To compute parameters $\hat{c}$ and $\hat{d}$ of the iMSP, recall the simple linear relationship $\rho_i = c * Z_i + d$, defining an over-determined set of linear equations in ρ_i and Z_i that can be solved for c and d. Solving this linear set of equations is equivalent to fitting a plane to a set of parallel lines in 3-D Euclidean space (Fig. 5), each having orientation θ_i. It is known that straightforward *least-squares* line fitting would be sensitive to outliers in the computed ρ_i values. The existence of such outliers is unavoidable in our case, due to pathology effects, digital image artifacts, and symmetry axis ambiguity in the higher brain slices. We perform a robust linear regression instead. The obvious choice is to use *least-median of squares* (LMS) [24], which has a breakdown point of 50%.[6]

After applying LMS regression, we identify (ρ_i, Z_i) outlier points by using the robust standard deviation measure defined in formula (12) (set $p = 2$) to filter points based on their residuals. A standard least-squares line fit is then applied to the inliers to compute a final estimate for $\hat{c}$ and $\hat{d}$ (see Fig. 6).

This final set of parameters $(\hat{a}, \hat{b}, \hat{c}, \hat{d})$ completely specify the best-fit iMSP. The roll angle of the head can now be estimated as $\hat{\phi} = -\arctan(\hat{c})$. Perpendicular distance of the iMSP from the origin of the ideal head coordinate system is computed as $\hat{d}\cos\hat{\phi}$. As a final step, we recompute a 2-D symmetry axis for each slice with orientation $\hat{\theta}$ and offset $\hat{\rho}_i = \hat{c} * Z_i + \hat{d}$. This is equivalent to intersecting the estimated iMSP with each brain slice to obtain a new set of 2-D symmetry axes.

6) iMSP Extraction Algorithm Summary:

Input: a set of brain scans in axial (or coronal) format, voxel dimensions.

Output: $\hat{a}, \hat{b}, \hat{c}, \hat{d}$, head yaw and roll angles $\hat{\theta}, \hat{\phi}$, translational offsets of the iMSP.

Algorithm (Fig. 7).

1) Isolate the head region. Reduce the size of each slice by smoothing and subsampling. Compute binary edge images $S_1, \ldots, S_n$ from the reduced slices.
2) Pick one of the lowest 2-D brain slices S_i. Construct $S_i' = S_i$ reflected w.r.t. $X = 0$ plane. Find $\theta_{init} = \arg\max\{C_i(S_i, rot(S_i', \theta))\}$ where C_i is the cross correlation of S_i and rotated S_i', and θ is sampled every 5° in the range of $[-90°, 90°]$ or $[-180°, 180°]$ if necessary.
3) find symmetry axis orientation θ_i on each 2-D slice S_i as $\theta_i = \arg\max\{C_i(S_i, rot(S_i', \theta_{init} + j))\}$, where j runs from -10 to 10° in 1° increments.
4) Compute the shared yaw (or roll) angle from all the axial (coronal) slices: $\hat{\theta} = robust(\theta_1, \ldots, \theta_n)$, where function $robust$ eliminates outliers [35] and finds the mean of the weighted inliers.
5) Compute image offsets ρ_i by finding the maximum cross correlation value of each yaw (roll)-angle-corrected 2-D slice and its vertical reflection.
6) Remove outliers from (ρ_i, Z_i) using least-median of squares line fitting [24] and then fit a least-squares line to the inliers using the equation $\rho_i = cZ_i + d$ to get $\hat{c}$ and $\hat{d}$.

[6]The breakdown point of an estimator is the fraction of outlying data points that may cause the estimator to take on an arbitrarily large aberrant value.

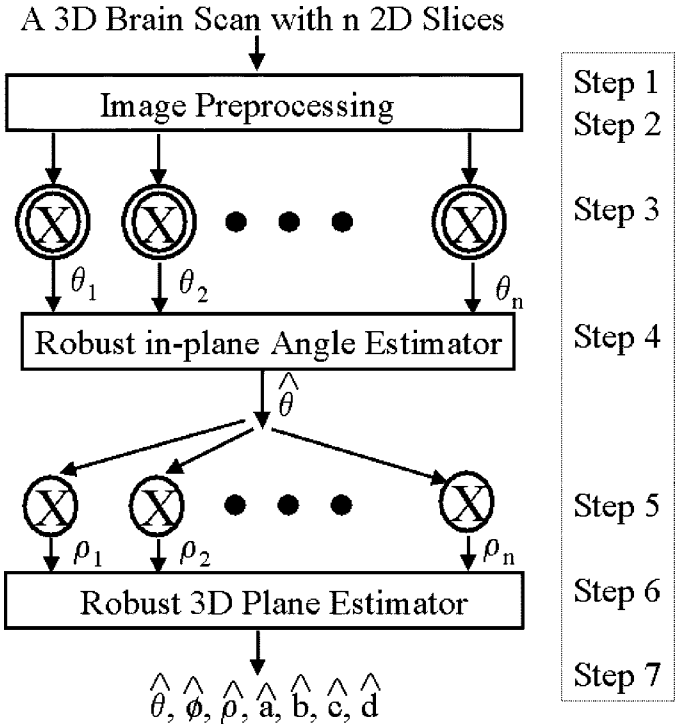

Fig. 7. A flow chart of the iMSP extraction algorithm, where "X" with a circle around it means 2-D cross correlation, and with a double circle means multiple cross correlations using different rotated images. The right column shows the corresponding step numbers described in the iMSP extraction algorithm.

7) Compute the remaining plane parameters $\hat{a} = \cos(\hat{\theta})$ and $\hat{b} = \sin(\hat{\theta})$, and roll angle $\hat{\phi} = -\arctan(\hat{c})$. Intersect the estimated MSP with each 2-D slice to obtain a new set of 2-D symmetry axes with orientation $\hat{\theta}$ and offset $\hat{\rho}_i = \hat{c} * Z_i + \hat{d}$.

IV. Implementation and Sample Results

The algorithm is implemented on an SGI[7] O2 R10000. using a mixture of MATLAB and C subroutines. The CPU time for running the algorithm is dominated by cross correlation computations. Each cross correlation takes 0.26 s for the 64 × 64 reduced-resolution slices used to estimate yaw angles, and 10 s for the original 512 × 512 slices used to estimate translational offset. Total time spent doing correlations for a 20-slice neural image is roughly 5 min. Total time for all algorithmic steps is roughly 7 min. No attention has been paid to speeding up the code, except for using the fast Fourier transform for cross correlation computation. The algorithm has been applied on 130 3-D image sets with varying modalities (CT [enhanced and nonenhanced] and MR [T1, T2, enhanced and nonenhanced]). Table II shows the parameters of a few sample input image sets. Note that some examples have very sparse sampling in the Z direction (every 10 mm). An automatically extracted "midsagittal" plane is shown in Fig. 2(b). Fig. 8 shows the symmetry axes extracted from a set of axial images with a roll angle of 15° (out-of-plane rotation). Figs. 1(b) and (d) and 9–11 show examples of extracted symmetry axes when there are obvious asymmetries in the head.

[7]Address: SGI, Mountain View, CA, 94043, USA. Website: http://www.sgi.com/o2/

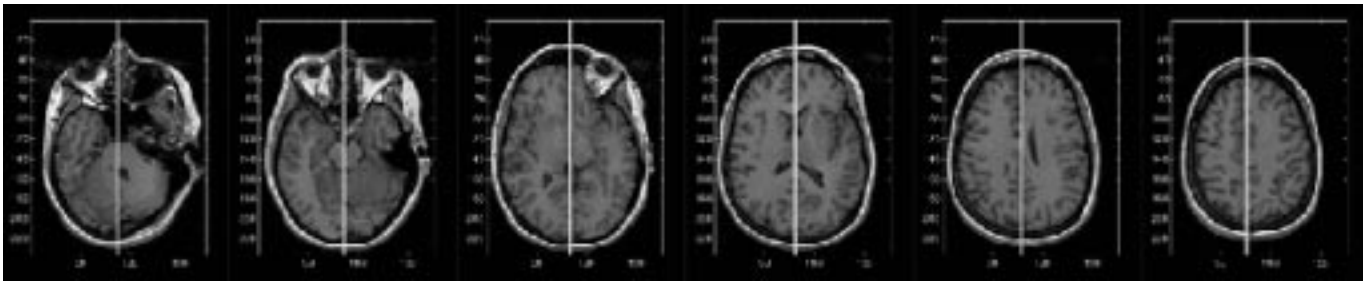

Fig. 8. The symmetry axes extracted from a set of MR axial slices with a 15° roll angle (out-of-plane rotation).

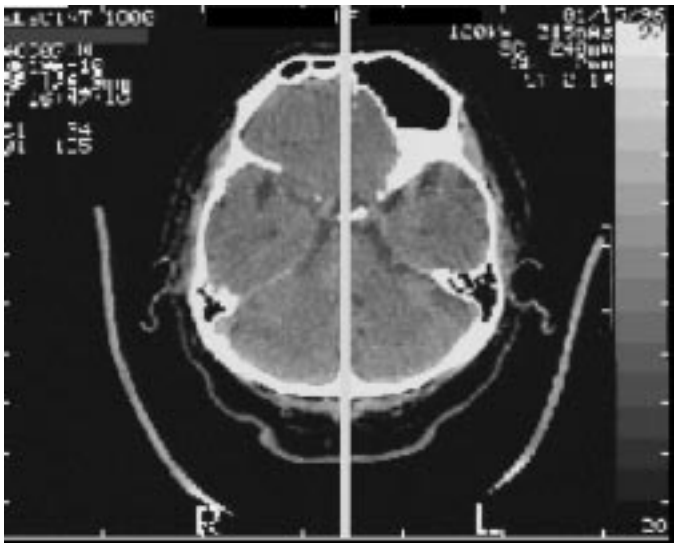

Fig. 9. The midsagittal plane automatically extracted from a clinical CT image where obvious asymmetry is present.

V. Evaluation

No obvious errors have been observed when applying the iMSP extraction algorithm to 130 clinical image sets with varying modalities and scan geometries. In this section, we report a series of experiments that test the robustness of the iMSP algorithm.

For the experiments in Sections V-B and V-C, we chose to construct an artificially symmetric image from clinical images for quantitative testing. This was done because 1) visual inspection is subjective; 2) from a real brain image, it is hard, if not impossible, to distinguish whether an error is caused by the iMSP algorithm or by the nonmodeled anatomic variations of human brains (see Section VI); 3) no human brain scan exhibits perfect digital symmetry, thus, no known ground truth in a real image can be used directly for iMSP algorithm evaluation.

Two ground truth image test sets were created from datasets 5 and 110, respectively (Table II); one is a dense, coronal MR volume, and the other is a sparse, axial CT volume. Each ground truth test set was constructed by finding the midsagittal plane by hand, then reflecting one half of the head volume about this midsagittal plane to form the other half, producing a perfectly symmetrical volume. Since the constructed test set is perfectly symmetric, the ground truth iMSP is known.

A. Yaw and Roll Angle Accuracy Evaluation

To evaluate the accuracy of computed yaw and roll angles, a densely sampled MR image set was resampled using trilinear interpolation to artificially vary the yaw angles from $-10°$ to $10°$ in $2.5°$ intervals, and the roll angles from $-15°$ to $15°$ in $5°$ intervals. To determine the approximate absolute ground truth angles of each dataset, we first ran the algorithm on the original dataset, revealing a yaw angle of $1.25°$ and a roll angle of $-1.75°$. These computed offsets of the original dataset were added to the known relative yaw and roll of each resampled dataset to determine a "ground truth" yaw and roll for that dataset. The algorithm was then run to determine an estimated yaw and roll angle. Given the above definition of ground truth, the average error was $<0.3°$ for computed yaw angles (Fig. 12) and $<0.75°$ for computed roll angles (Fig. 13).

B. Tolerance to Asymmetry

To test the sensitivity of the iMSP extraction algorithm to lesions of varying size and position, we constructed a perfectly symmetrical volumetric neuroimage from a clinical CT scan of a normal brain (dataset 110 in Table II). Spherical "lesions" are superimposed in the symmetrical volumetric image by specifying a 3-D position, radius and intensity value. The lesion intensity replaces the densities in the CT scan. Fig. 14 shows one result of iMSP extraction for a lesion with radius 42.97 mm (100 pixels), with density darker than the surrounding tissues. We have tested the algorithm extensively with lesions in different locations, and have "grown" lesions of up to 128.9 mm (300 pixels) in radius. The iMSP algorithm's performance starts to decline when the tumor radius reaches 85.9 mm (200 pixels), see Fig. 15, and totally fails when the lesion radius reaches 107.4 mm (250 pixels), as is summarized by the plots in Fig. 16. For comparison, the average radius of a human brain is approximately 70 mm.

C. Comparison of IMSP Extraction Methods: Intensity-Based Versus Edge-Based

In this section, we compare our iMSP with a representative intensity-based approach: maximization of mutual information (MI). The iMSP is extracted using MI by registering a 3-D brain volume V with a reflected version of itself V'. Following the same geometric reasoning as in Section III, halving the transformation parameters provides the solution for the location of

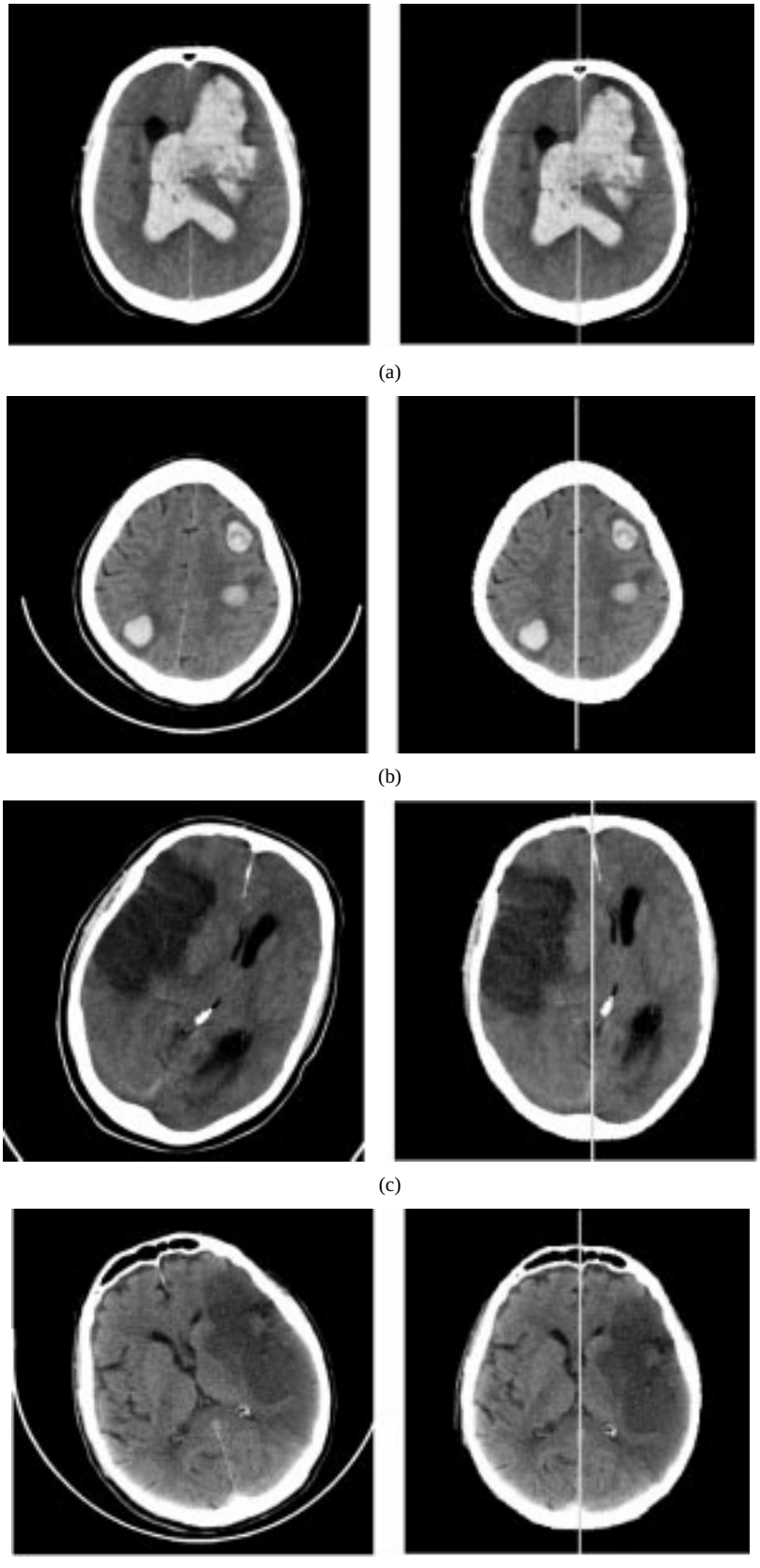

Fig. 10. The symmetry axes extracted from different clinical CT scans where obvious asymmetry is present. (a) Acute blood (left frontal), (b) multifocal acute blood (left frontal and right parietal), (c) infarct (right frontal), and (d) infarct (left frontal and temporal).

the best reflection plane. The mutual information registration code implemented in [18] is used for this testing.

1) Tolerance to Noise and Asymmetry: To study the effects of noise and asymmetry on iMSP extraction, we have tested our

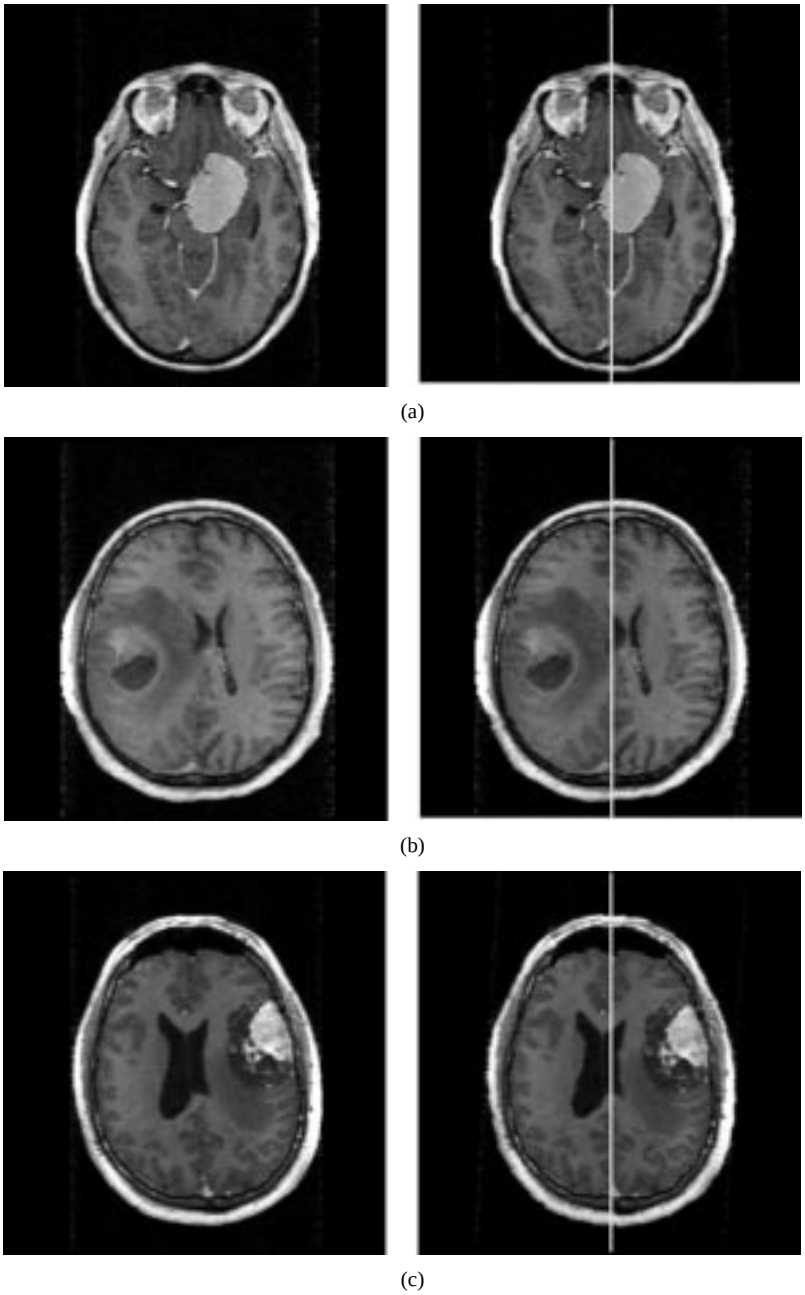

Fig. 11. Sample MR tumor images with iMSP identified. Input images are originally in sagittal slices. Images courtesy of Dr. Kikinis, Harvard Medical School. Pathology types: (a) meningioma (left parasellar), (b) astrocytoma (right frontal), and (c) astrocytoma (left frontotemporal).

algorithm on the MR ground truth dataset, side-by-side with the MI-based approach. The data is artificially degraded by adding different levels of zero-mean Gaussian noise, and by inserting spherical lesions of varying diameters. Algorithm breaking points are determined by incrementally adding noise until each respective algorithm fails to detect the correct symmetry plane. Each incremental addition of noise corresponds to a loss of 6.02 dB of signal-to-noise ratio (SNR), or roughly 1 bit of information.[8] Fig. 17 shows representative resulting slices, and iMSPs extracted by the algorithms (shown on 2-D slices). In both cases, with and without lesions, the MI-based approach fails at lower levels of noise than our edge-based approach (Fig. 17). The algorithm reported in this paper worked correctly at levels of noise up to SNR $= -10.8$ dB when no lesion was present, and up to SNR $= -4.82$ dB in the presence of a lesion with radius 56.25 mm (60 pixels).

2) Tolerance to Bias Field: We have also tested both our iMSP algorithm and the MI-based approach on MRI volumes corrupted by a simulated intensity "bias field" (Fig. 18). A synthetic bias field is generated as a Gaussian with sigma $=$ 70 pixels, centered at pixel offset (X, Y), rescaled so that the intensity at pixel (X, Y) has grey level G. This bias image is then added to each slice of the MRI volume. Testing was performed for different values of G, ranging from a mild bias field ($G = 0.25$ times the maximum grey value Gmax in the original MRI volume), to very severe ($G = 10 \times$ Gmax). The

[8]SNR is defined as $10 * \log$(var(signal)/var(noise)). An SNR of less than zero means that the noise has a higher variance than the signal.

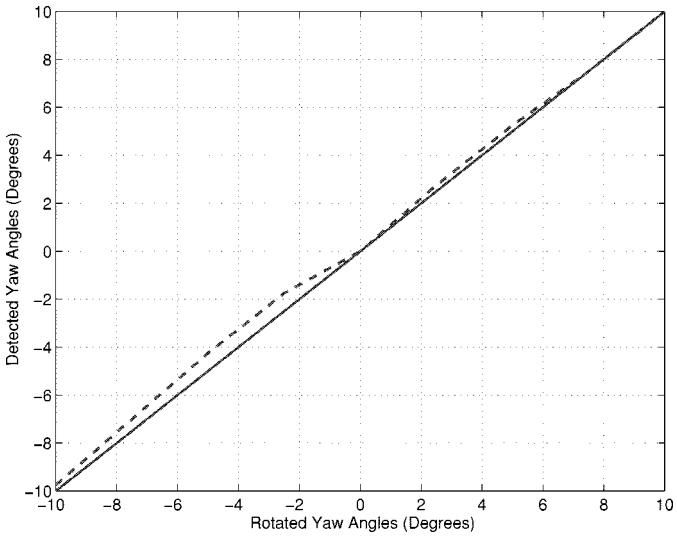

Fig. 12. Actual versus detected yaw angles in the MR axial scans. The solid line is the perfect detection result and the dashed line is formed from the yaw angle values detected using our algorithm.

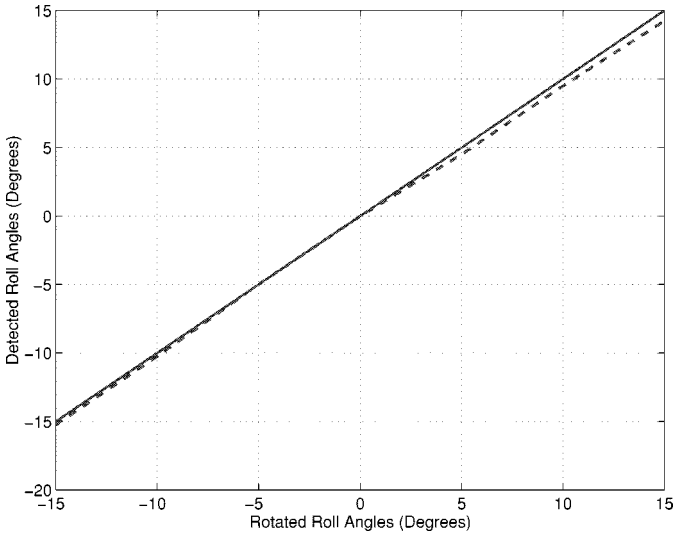

Fig. 13. Actual versus detected roll angles in the MR coronal scans. The solid line is the perfect detection result and the dashed line is formed from the roll angle values detected using our algorithm.

mutual information approach failed when even the mildest bias was present [Fig. 18(a)]. In contrast, our algorithm did not fail at even the highest levels of bias field tested [Fig. 18(b)]. This is so because our method is based on local edge detection, which is relatively unaffected by the addition of a smooth intensity bias field, while the global distribution of intensity values in the volume is critically important to the mutual information approach.

D. Comparison with Human Experts

To compare the algorithm with human performance, we asked two neuroradiologists to hand-draw the ideal midline on each 2-D slice of six randomly chosen 3-D CT brain scans. The experience in interpreting clinical CT images of the first and the second medical doctors is 20 and 4.5 years, respectively. The radiologists were allowed to view the whole set of 2-D slices from one volumetric image for reference while using a mouse to click on a brain scan displayed directly on a computer screen. The fairness of this comparison between a human expert (drawing a line on each 2-D slice) and the computer algorithm (fitting a plane within the whole 3-D image) is based on the fact that, when interviewed, the neuroradiologists acknowledged "We are actually at an equivalent stage as the computer algorithm in that when we are drawing the midline, we have a mental picture of the 3-D brain. This mental picture is formed by looking at all the 2-D slices, and drawing upon many years of experience." Although geometric reasoning tells us that the angles of the intersection line of the iMSP and each axial slice should be the same (Section III-A), there is a variation in the angles determined by the human experts. The standard deviation of the human measurement error on different sets of slices varies from 0.5595° to 2.3678° (Table III).

The correlation scores between Experts 1 and 2, Expert 1 and the computer algorithm, and Expert 2 and the algorithm are, respectively, 0.9968, 0.9951, and 0.9874. Thus, there is a high level of agreement between the human experts, and between each expert and our algorithm. This can also be seen by plotting points representing one agent's estimates (there being three agents—two humans, and one computer) against another's, as in Fig. 19. In each case, the data points lie very close to the superimposed least squares line $Y = \alpha + \beta X$. Indeed, the F-tests for the three regressions [4] were highly significant: 619.5, 407.8, and 155.19, respectively, all in one and four degrees of freedom. This indicates that the angles estimated by all three agents are very similar to each other. In all three cases, the estimate of α from the least squares line is not significantly different from zero, at level 0.05, and all three confidence intervals for β include 1 ([0.8278, 1.0356], [0.7804, 1.0292], and [0.7464, 1.1745]). Therefore, there is no statistically significant difference between the estimates given by the three agents.

VI. Discussion

We have observed that iMSP computation is not adversely affected by large lesions and mass effect in pathological images. This may seem strange since cross correlation is used as a measure for matching two images (in our case, the two halves of a brain). It is natural to ask why the algorithm works so well on drastically asymmetrical images. We can provide the following relevant observations:

1) *Majority Rules:* For a 3-D pathological brain, a lesion resides on only a relatively small number of 2-D slices; thus, when the iMSP is fit to the whole set of 2-D slices, normal slices with prominent bilateral symmetry dominate the iMSP's position.
2) *Edge Features:* By using edge features rather than the original intensity images directly, the effect of strong density concentration around lesions is much reduced.
3) *Lower Brain Slice Stability:* Lower brain slices are relatively stable due to the bilateral structure of the skull.

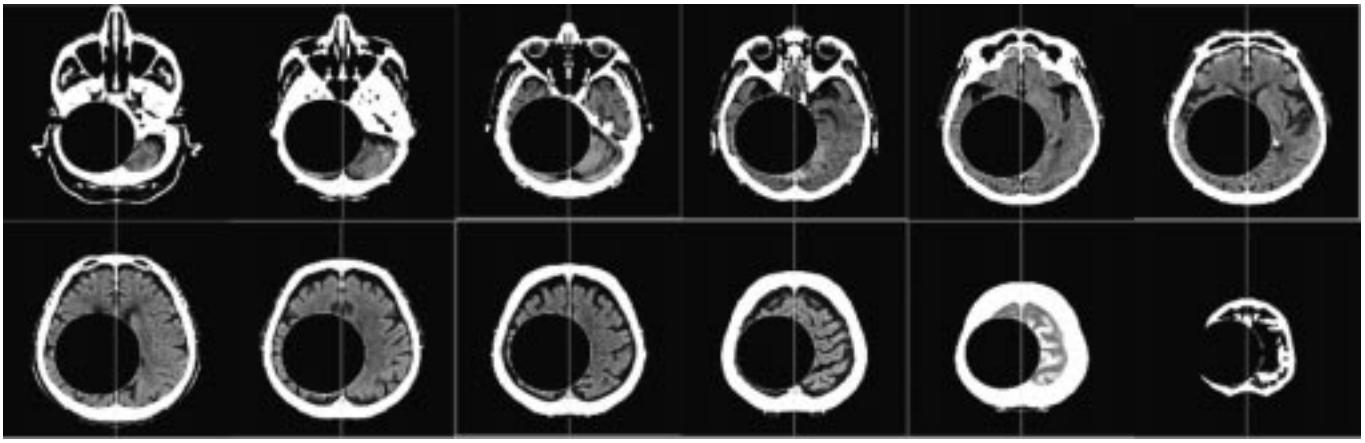

Fig. 14. The iMSP algorithm performs successfully when presented with an artificially grown lision of 42.77 mm (100 pixels) radius.

Fig. 15. The iMSP algorithm performance on an artificial lesion with 85.5 mm (200 pixels) radius.

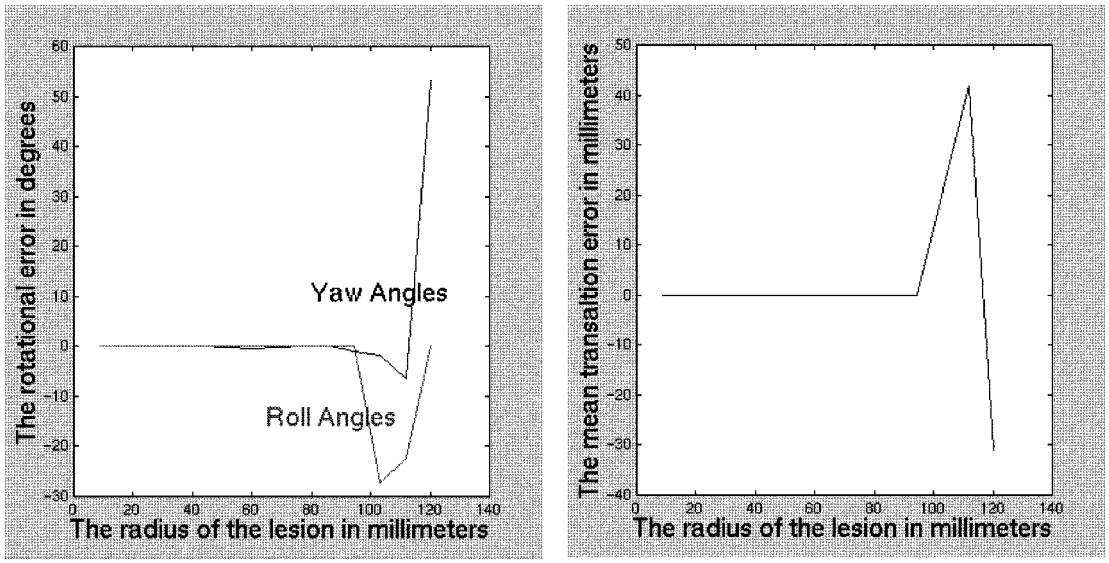

(a) (b)

Fig. 16. (a) Yaw and roll angle errors and (b) translational offset errors versus the radius of an artificial lesion in millimeters, (1 pixel = 0.4297 mm). The spherical lesion is centered at the 3-D image pixel location $X = 310$, $Y = 210$, and $Z = 350$ (that is the point [$X = 133$ mm, $Y = 90$ mm, and $Z = 150$ mm] with respect to the back-upper-left corner of the image volume). The iMSP algorithm's performance starts to decline when the tumor radius reaches 86 mm (200 pixels), and totally fails when the lesion radius reaches 107.4 mm (250 pixels).

In our algorithm, the lower brain slices are given more weight when determining the orientation of the iMSP.

4) *Robust Estimators:* Robust estimation techniques are used to remove outliers from computed measurements before combining them to determine other quantities.
5) *Brain Structure:* Although the bony skull is influential, the accuracy of the detected symmetry axes decreases when the symmetry axes are determined by the silhouette of the skull alone [14]. Therefore, the internal structure of the brain appears to enhance the position and orientation accuracy. This brain structure is emphasized by using edge features.

This work addresses two main issues. One is that the brain sometimes departs drastically from perfect symmetry. The other is that using clinical images introduces challenging factors like large initial offsets, undersampling, artifacts (bias field) and noise. The acute advantage of our iMSP extraction algorithm over existing MSP extraction algorithms is its robust treatment

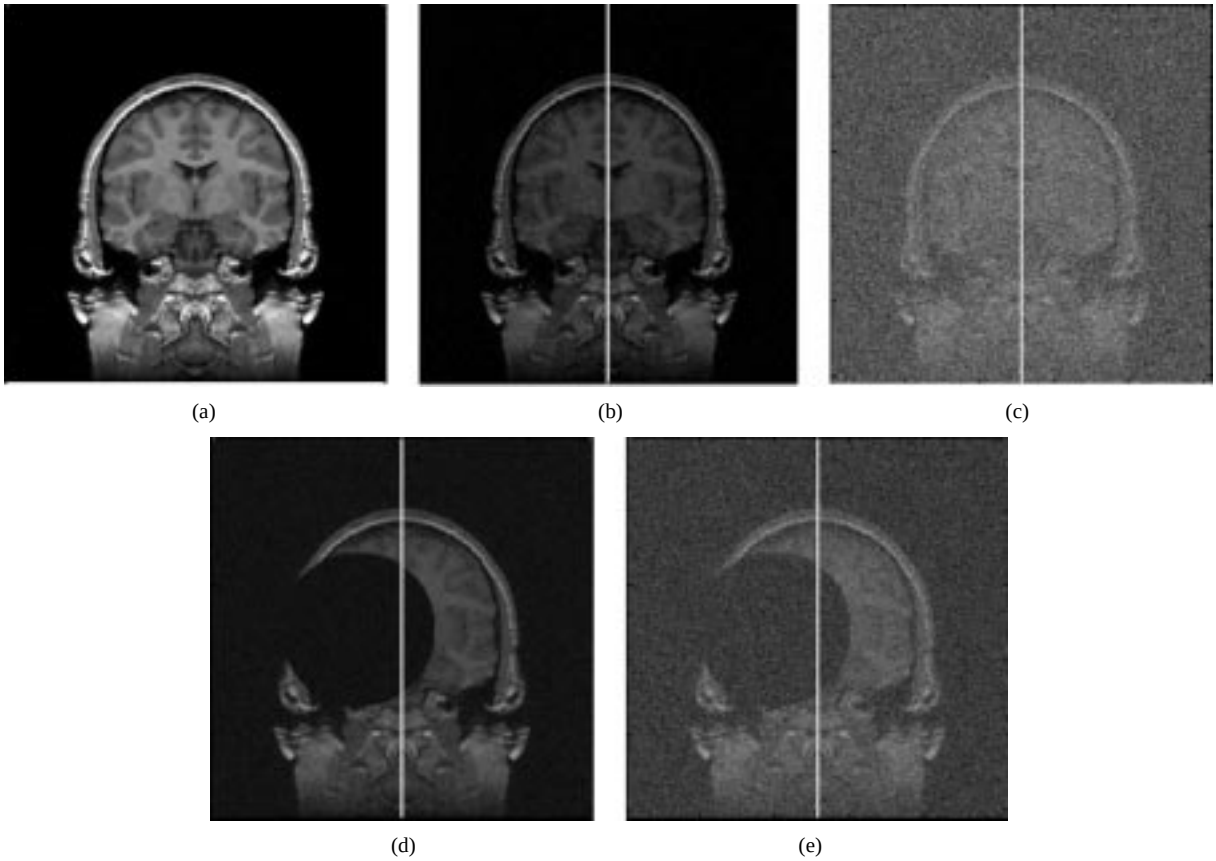

Fig. 17. Sample results on images artificially degraded with lesions and noise, to determine algorithm breaking points. The images shown with iMSP identified are the ones just before the corresponding algorithm's breaking point. (a) One slice from original dataset with no noise, SNR = 43.35 dB. (b) Result from iMSP extraction using MI-based registration, on a dataset with added noise only. SNR of breaking point is 7.23 dB. (c) Result from our algorithm when run on a dataset with added noise only. SNR of breaking point is −10.84 dB. (d) Result from iMSP extraction using MI-based registration, on a dataset with lesion (radius = 56 mm, about 60 pixels) plus noise. SNR of breaking point is 13.25 dB. (e) Result from our algorithm, on a dataset with lesion (same) plus noise. SNR of breaking point is −4.82 dB.

of unevenly sampled, anisotropic clinical images, particularly CT images, containing large lesions and mass effect.

Limitations of this iMSP extraction algorithm include:

a) "Ideal midsagittal plane is a planar surface" Assumption: It is under this assumption that geometric reasoning tells us that the yaw (roll) angle on each slice of an axial (coronal) set should be the same [see (3)]. Sometimes this assumption is violated by true anatomical structure. This is exactly where a clean mathematical model and complicated reality may conflict with each other. Even for normal human brains, the interhemispherical plane may sometimes be a curved surface (for example, similar to the shape of a piece of a potato chip); therefore, a plane cutting through the brain will not always intersect each 2-D axial (coronal) slice coincident with the "midline" of the 2-D slice. If the goal is to find a reference plane, then the coincidence issue is not important so long as the iMSP can be extracted consistently. If the goal is to find the exact shape of the interhemispherical membrane, then the extracted iMSP can be used as the initial position for an energy minimizing procedure [e.g., Fig. 1(d)].

b) Out-of-plane rotation: When out-of-plane rotation is larger than 20°, estimates of the roll (yaw) angle from a stack of axial (coronal) slices can not be trusted. This is because the ρ_is, the offsets of the midline, can be under-estimated, causing the roll (yaw) angle value to be smaller than it is in reality. One strategy used to increase robustness to large out-of-plane rotation errors is to use both axial and coronal slices simultaneously to estimate the yaw and roll angles (usually, one of these sets of slices is measured directly, and the other is created by resampling the image volume). Since there is no limit to in-plane rotation angle estimation, the same algorithm described in Section III-B can run on both orientations in parallel, with the computed result of the in-plane rotation angles (the computed yaw angle from axial slices or the computed roll angle from coronal slices) weighted more highly than the out-of-plane rotation angle estimates.

c) Speed: Cross correlation is an expensive operation in general. We have not made any special effort to speed up the algorithm other than using the fast Fourier transform (Section IV). When a 3-D image contains a large number of slices, the iMSP computation process can be slow. However, from Fig. 7 one can see that the cross correlation operation for each 2-D slice can be done in parallel instead of sequentially. If a parallel hardware device such as an optical correlator were used, the speed of this algorithm would be greatly increased.

VII. Conclusion

In this paper, we have presented an iMSP extraction algorithm that is capable of finding the ideal MSP from asymmetrical neural images without compromising accuracy on sym-

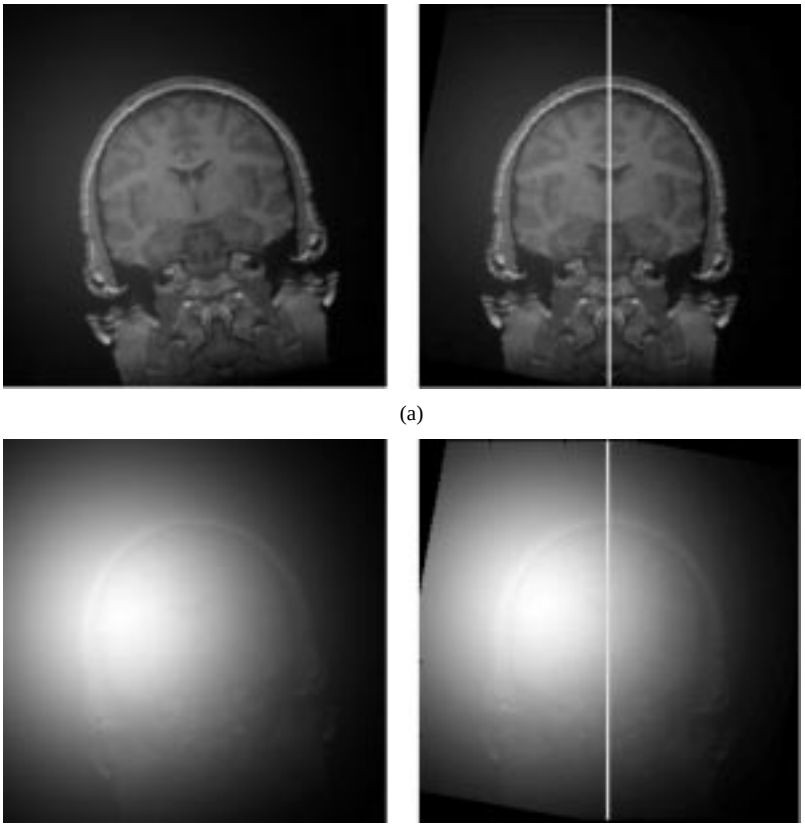

Fig. 18. Sample results on images with artificially added bias field. The original MR test image can be found in Fig. 17(a). Here, the roll angle of each test image is set to 10°. (a) The MR test image with added bias field $G = 0.25$, and the iMSP found by our algorithm. The algorithm based on maximization of mutual information failed on this test case. (b) The MR test image with added bias field $G = 10$, from which our algorithm still finds the iMSP correctly.

TABLE III
COMPARISON OF HUMAN VERSUS COMPUTER-ESTIMATED YAW ANGLES (IN DEGREES)

Label	Pathology	# Slices	Expert 1 Mean(θ_i)	Expert 2 Mean(θ_i)	Expert 1 Std(θ_i)	Expert 2 Std(θ_i)	Computed Yaw $\hat{\theta}$
CMU121	infarct	17	1.6208	1.5730	1.0290	0.9972	0.8202
CMU126	blood	21	7.1404	6.2472	2.3678	0.5595	6.0347
CMU129	infarct	10	-2.0248	-1.8201	1.1141	1.6304	-2.2318
CMU130	blood	21	1.3257	0.6829	0.9091	0.8967	1.3216
CMU170	normal	20	-4.3187	- 4.5296	1.2781	2.0080	-4.5109
CMU171	normal	22	-1.3028	- 1.7582	1.0626	1.1963	-1.0129

metrical ones. Our work presents a sound geometric method for estimating the symmetry of a 3-D object using a sparse set of 2-D slices. The proposed algorithm has been applied to 130 clinical image sets with varied modality, volumetric sampling, and background clutter. In this paper, the algorithm has been quantitatively evaluated using three methods: 1) image resampling, 2) introduction of spherical lesions, noise and simulated bias-fields, and 3) comparison with human experts. The detection accuracy of yaw and roll angles on the resampled images are estimated within 1° of rotated angle values. The iMSP estimation method does not begin to break down until lesions occupy a significant fraction of the brain, SNR is very low, or the bias field is quite intense. Finally, no statistically significant difference can be found between yaw angles estimated by the algorithm and those estimated by trained neuroradiologists. The iMSP algorithm has also been compared with an approach based on maximization of mutual information registration, and has been found to exhibit superior performance under adverse conditions.

The robustness and simplicity of this approach stems from using edge information rather than direct use of intensities, using a sound mathematical model of 2-D-3-D imaging geometry, and using robust parameter estimation techniques to remove the effects of outliers. This work combines 2-D and 3-D images in such a way that 2-D data is used to predict a 3-D plane and the 3-D structure is used to correct local errors on 2-D slices.

We are currently exploring how to use the iMSP extraction algorithm to facilitate registration and comparison of brain images from multiple sources and modalities. Computing similarity among diverse brain images is part of an ongoing project to study how a patient's brain scan can be used to retrieve medically relevant cases from a neural image database [16], [17]. Other future work includes choosing a good statistical sampling

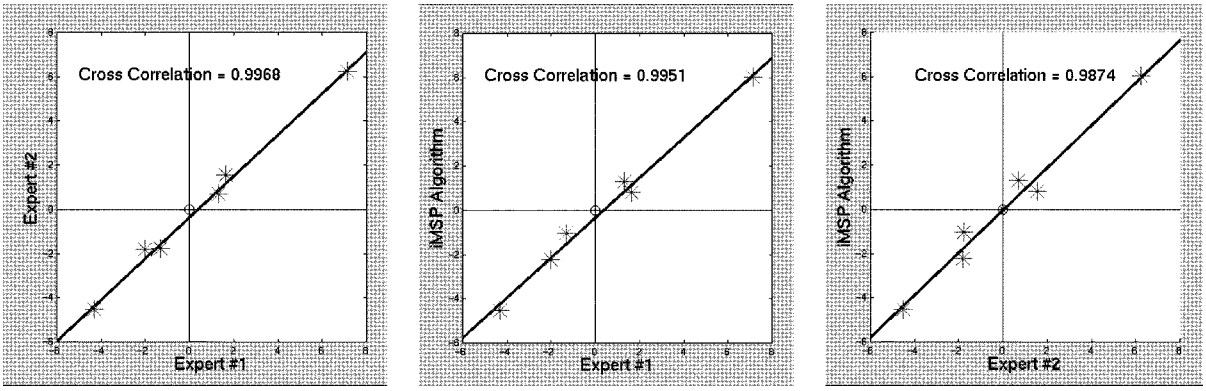

(a) (b) (c)

Fig. 19. The least-squares linear regression lines $Y = \alpha + \beta X$ for pairwise comparison of experts and the iMSP algorithm. The estimated α, β values are, respectively, (a) $\alpha_{12} = -0.3131$, $\beta_{12} = 0.9317$; (b) $\alpha_{13} = -0.2979$, $\beta_{13} = 0.9048$; (c) $\alpha_{23} = 0.0069$, $\beta_{23} = 0.9605$, where the subscripts denote 1: Expert 1, 2: Expert 2, and 3: the iMSP algorithm. In all three cases, the estimate of α is not significantly different from zero, at level 0.05, and all three confidence intervals for β include 1 ([0.8278, 1.0356], [0.7804, 1.0292], [0.7464, 1.1745]).

method for dense 3-D brain images, evaluation of the iMSP extraction algorithm on orthopedic images, and testing the effectiveness of this approach on image modalities such as PET and SPECT.

ACKNOWLEDGMENT

The authors would like to thank Dr. R. Kikinis (M.D.) of Harvard Medical School for providing MR tumor images, Dr. F. Maes for providing the mutual information registration code, and Dr. N. Lazar (Statistics Department, Carnegie Mellon University) and Dr. G. Gordon (Burning Glass Technologies) for verifying statistical tests results reported in this paper. The authors would also like to thank our anonymous reviewers and our Associate Editor, Dr. D. J. Hawkes, for helping to improve this paper.

REFERENCES

[1] B. Ardekani, J. Kershaw, M. Braun, and I. Kanno, "Automatic detection of the mid-sagittal plane in 3-D brain images," *IEEE Trans. Med. Imag.*, vol. 16, pp. 947–952, Dec. 1997.

[2] M. E. Brummer, "Hough transform detection of the longitudinal fissure in tomographic head images," *IEEE Trans. Med. Imag.*, vol. 10, pp. 74–81, Feb. 1991.

[3] J. Canny, "A computational approach to edge detection," *IEEE Trans. Pattern Anal. Machine Intell.*, vol. PAMI-8, pp. 679–698, June 1986.

[4] G. Casella and R. L. Berger, *Statistical Inference*. Belmont, CA: Duxbury Press, 1990.

[5] T. J. Crow, "Schizophrenia as an anomaly of cerebral asymmetry," in *Imaging of the Brian in Psychiatry and Related Fields*, K. Maurer, Ed. Berlin, Germany: Springer-Verlag, 1993.

[6] R. J. Davidson and K. Hugdahl, Eds., *Brain Asymmetry*. Cambridge, MA: MIT Press/Bradford Books, 1996.

[7] V. Di Gesu and C. Valenti, "Symmetry operators in computer vision," *Vistas Astron.*, vol. 40, no. 4, pp. 461–468, 1996.

[8] J. S. Duncan and N. Ayache, "Medical image analysis: Progress over two decades and the challenges ahead," *IEEE Trans. Pattern Analysis and Machine Intelligence*, vol. 22, no. 1, pp. 85–106, 2000.

[9] P. J. Flynn, "3-D object recognition with symmetric models: Symmetry extraction and encoding," *IEEE Trans. Pattern Anal. Machine Intell.*, vol. 16, pp. 814–818, Aug. 1994.

[10] N. Geschwind and W. Levitsky, "Human brain: Left–right asymmetries in temporal speech region," *Science*, vol. 161, pp. 186–187, 1968.

[11] R. Guillemaud, P. Marais, A. Zisserman, T. J. Mc Donald, and B. Crow, "A 3-Dimensional midsagittal plane for brain asymmetry measurement," *Schizophrenia Res.*, vol. 18, no. 2–3, pp. 183–184, 1995.

[12] L. Junck, J. G. Moen, G. D. Hutchins, M. B. Brown, and D. E. Kuhl, "Correlation methods for the centering, rotation, and alignment of functional brain images," *J. Nucl. Med.*, vol. 31, no. 7, pp. 1220–1226, July 1990.

[13] Y. Liu, R. T. Collins, and W. E. Rothfus, "Evaluation of a robust mdisagittal plane extraction algorithm for coarse, pathological 3-D images," in *Proc. Medical Imaging Computing and Comptuer Assisted Intervention (MICCAI 2000)*, S. L. Delp, T. DiGioia, and G. Jaramaz, Eds., Pittsburgh, PA, Oct. 2000, pp. 81–94.

[14] Y. Liu, R. T. Collins, and W. E. Rothfus, "Automatic extraction of the central symmetry (mid-sagittal) plane from neuroradiology images," Carnegie Mellon Univ., Pittsburgh, PA, The Robotics Institute, Tech. Rep. CMU-RI-TR-96-40, 1996.

[15] ——, "Automatic bilateral symmetry (midsagittal) plane extraction from pathological 3-D neuroradiological images," in *Proc. SPIE Int. Symp. Medical Imaging*, vol. 3338, San Diego, CA, Feb. 1998, pp. 1528–1539.

[16] Y. Liu and F. Dellaert, "A classification-based similarity metric for 3-D image retrieval," in *Proc. Computer Vision and Pattern Recognition Conf.*, Santa Barbara, CA, June 1998, pp. 800–805.

[17] Y. Liu, W. Rothfus, and T. Kanade, "Content-based 3-D neuroradiologic image retrieval: Preliminary results," in *Proc. IEEE Workshop Content-Based Access of Image and Video Libraries, in Conjunction with Int. Conf. Computer Vision*, Bombay, India, Jan. 1998, pp. 91–100.

[18] F. Maes, A. Collignon, D. Vandermeulun, G. Marchal, and P. Suetens, "Multimodality image registration by maximization of mutual information," *IEEE Trans. Med. Imag.*, vol. 16, pp. 187–198, Apr. 1997.

[19] T. Masuda, K. Yamamoto, and H. Yamada, "Detection of partial symmetry using correlation with rotated-reflected images," *Pattern Recogn.*, vol. 26, no. 8, pp. 1245–1253, 1993.

[20] S. Minoshima, K. L. Berger, K. S. Lee, and M. A. Mintum, "An automated method for rotational correction and centering of three-dimensional functional brain images," *J. Nucl. Med.*, vol. 33, no. 8, pp. 1579–1585, August 1992.

[21] S. Prima, S. Ourselin, and N. Ayache, "Computation of the mid-sagittal plane in 3-D images of the brain," in *Proc. 6th Eur. Conf. Computer Vision*, Dublin, Ireland, 2000, pp. 685–701.

[22] D. Reisfeld, H. Wolfson, and Y. Yeshurun, "Context free attentional operators: The generalized symmetry transform," *Int. J. Comput. Vis.*, vol. 14, pp. 119–130, 1995.

[23] A. Rosenfeld and A. C. Kak, *Digital Picture Processing*. New York: Academic, 1976.

[24] P. J. Rousseeuw, "Least median-of-squares regression," *J. Amer. Stat. Assoc.*, vol. 79, pp. 871–880, 1984.

[25] J. C. Russ, *The Image Processing Handbook*. Boca Raton, FL: CRC, 1992.

[26] D. Shen, H. H. S. Ip, K. T. Cheung, and E. K. Teoh, "Symmetry detection by generalized complex (gc) moments: A close-form solution," *IEEE Trans. Pattern Anal. Machine Intell.*, vol. 21, pp. 466–476, May 1999.

[27] S. Smith and M. Jenkinson, "Accurate robust symmetry estimation," in *Proc. Medical Image Computing and Computer-Assisted Intervention—MICCAI'99*, Cambridge, U.K., 1999, pp. 308–317.

[28] C. Studholme, D. L. G. Hill, and D. J. Hawkes, "Automated 3-D registration of MR and CT images of the head," *Med. Image Anal.*, vol. 1, no. 2, pp. 163–175, June 1996.
[29] C. Sun, "Symmetry detection using gradient information," *Pattern Recogn. Lett.*, vol. 16, no. 9, pp. 987–996, 1995.
[30] J. Talairach and P. Tournoux, *Co-Planar Steriotaxic Atlas of the Human Brain*. New York: Thieme Medical, 1988.
[31] P. Viola and W. Wells III, "Alignment by maximization of mutual information," in *Proc. ICCV95*, Cambridge, MA, 1995, pp. 16–23.
[32] R. Waltzman, "Finding symmetries of polyhedra," Center for Automation Research, Univ. Maryland, College Park, Tech. Rep. CAR-TR-333, CS-TR-193, 1987.
[33] W. M. Wells III, P. Viola, H. Atsumi, S. Nakajima, and R. Kikinis, "Multi-modal volume registration by maximization of mutual information," *Med. Image Anal.*, vol. 1, no. 1, pp. 35–51, March 1996.
[34] J. D. Wolter, T. C. Woo, and R. A. Volz, "Optimal algorithms for symmetry detection in two and three dimensions," in *The Visual Computer*. New York: Springer-Verlag, 1985.
[35] Z. Zhang, "Parameter Estimation Techniques: A Tutorial with Application on Conic Fitting," *Image Vis. Computing*, vol. 15, pp. 59–76, 1997.